Observed Relationships between Sea Surface Temperature, Vertical Wind Shear, Tropical Organized Deep Convection, and Radiative Effects

WEI-TING HSIAO,[a] ERIC D. MALONEY,[a] NICOLAS M. LEITMANN-NIIMI,[a,b] AND CHRISTIAN D. KUMMEROW[a]

[a] *Department of Atmospheric Science, Colorado State University, Fort Collins, Colorado*
[b] *NASA Goddard Institute for Space Studies, New York, New York*

(Manuscript received 3 May 2023, in final form 13 November 2023, accepted 6 December 2023)

ABSTRACT: Organized deep convective activity has been routinely monitored by satellite precipitation radar from the Tropical Rainfall Measuring Mission (TRMM) and Global Precipitation Mission (GPM). Organized deep convective activity is found to increase not only with sea surface temperature (SST) above 27°C, but also with low-level wind shear. Precipitation shows a similar increasing relationship with both SST and low-level wind shear, except for the highest low-level wind shear. These observations suggest that the threshold for organized deep convection and precipitation in the tropics should consider not only SST, but also vertical wind shear. The longwave cloud radiative feedback, measured as the tropospheric longwave cloud radiative heating per amount of precipitation, is found to generally increase with stronger organized deep convective activity as SST and low-level wind shear increase. Organized deep convective activity, the longwave cloud radiative feedback, and cirrus ice cloud cover per amount of precipitation also appear to be controlled more strongly by SST than by the deviation of SST from its tropical mean. This study hints at the importance of non-thermodynamic factors such as vertical wind shear for impacting tropical convective structure, cloud properties, and associated radiative energy budget of the tropics.

SIGNIFICANCE STATEMENT: This study uses tropical satellite observations to demonstrate that vertical wind shear affects the relationship between sea surface temperature and tropical organized deep convection and precipitation. Shear also affects associated cloud properties and how clouds affect the flow of radiation in the atmosphere. Although how vertical wind shear affects convective organization has long been studied in the mesoscale community, the study attempts to apply mesoscale theory to explain the large-scale mean organization of tropical deep convection, cloud properties, and radiative feedbacks. The study also provides a quantitative observational baseline of how vertical wind shear modifies cloud radiative effects and convective organization, which can be compared to numerical simulations.

KEYWORDS: Deep convection; Wind shear; Sea surface temperature; Cloud radiative effects; Satellite observations; Tropical variability

1. Introduction

Tropical precipitation is largely produced by convection that can be classified into certain types, each of them imposing distinct moistening and heating effects on the atmospheric vertical profile (e.g., Johnson et al. 1999; Elsaesser et al. 2010; Houze et al. 2015; Chen et al. 2021). Long-lived, horizontally widespread *organized* deep convection dominates the spatiotemporal distribution of the precipitation means and extremes in the current climate, and will regulate how these change with climate warming (Rossow et al. 2013; Tan et al. 2015; Roca and Fiolleau 2020; Semie and Bony 2020). Instead of being a passive factor in how tropical precipitation is statistically realized, organized deep convection drives radiative effects that not only locally help maintain its own development, but also regulate Earth's energy budget through modification of moisture, cloudiness, and large-scale circulation (Houze 1989; Schumacher et al. 2004; Bony et al. 2016, 2020). Differences in simulating organized deep convection and related processes in tropical ascending regions have been suggested to contribute to a spread in future climate projections (Bony et al. 2015; Mauritsen and Stevens 2015; Wolding et al. 2020; Lee et al. 2022). Thus, it is vital to understand what controls the activity of organized deep convection in the tropics.

Sea surface temperature (SST) has been previously shown to strongly regulate tropical deep convection and precipitation. Early pioneering studies showed positive correlations between tropical SST and deep convective activity as measured by outgoing longwave radiative flux, with a "pick-up" of convective activity above SSTs of 26°–27°C observed (Gadgil et al. 1984; Graham and Barnett 1987; Waliser and Graham 1993; Zhang 1993; Lau et al. 1997). Studies utilizing cloud-resolving models have shown SST thresholds for the onset of aggregated convection, a numerical phenomenon possibly relevant to real-world organized deep convection, but this dependence is sensitive to the model and simulation setup (Wing et al. 2017; Wing 2019; Wing et al. 2020). In addition, observations suggest that higher precipitation is collocated with higher SST relative to the tropical mean (SST^*) (Sobel et al. 2002), associated with higher convective

Supplemental information related to this paper is available at the Journals Online website: https://doi.org/10.1175/JCLI-D-23-0262.s1.

Corresponding author: Wei-Ting Hsiao, weiting.hsiao@colostate.edu

DOI: 10.1175/JCLI-D-23-0262.1

instability (Vecchi and Soden 2007) and column saturation fraction (CSF) (Bretherton et al. 2004), both of which imply higher effective buoyancy to support convective systems. While modern observation has started to support global surveys of convective systems (e.g., Zipser et al. 2006; Houze et al. 2015), studies that explicitly examine the observed relationship between tropical SST or SST^* and organized deep convection are sparse.

In addition to SST and its correlated thermodynamic factors, organized deep convection can be impacted by nonthermodynamic factors. It has long been recognized by the mesoscale meteorology community that the presence of low-level wind shear assists in the development of mesoscale convective systems (Houze 2004, and references therein). For instance, low-level wind shear balances the horizontal vorticity created by convective cold pools, which helps support the growth of new convective cells in a convection system (Rotunno et al. 1988). In numerical experiments, the relationship between convective aggregation and vertical wind shear is complicated, probably due to different simulation setups among studies (Bretherton et al. 2005; Abbot 2014; Tsai and Wu 2017; Wing et al. 2017). In observations, low-level vertical wind shear in the preinitiation stage of convection has been shown to favor organized deep convection in regional survey studies, consistent with mesoscale theory (Laing and Fritsch 2000). These different results imply a need for validation from an observational-based, global-coverage investigation of the relationship between vertical wind shear and tropical organized convection, and how thermodynamic factors jointly affect this relationship.

This study aims to improve the understanding of how not only thermodynamic but also large-scale dynamic conditions impact the statistical properties of tropical convective organization and associated radiative effects. The quantitative assessment of the observed connections between organized deep convection, radiative effects, precipitation, SST, and low-level wind shear in the tropics can be used to evaluate biases in numerical simulations, and also provide basic insight into the dynamics of large-scale convective modes of variability in the tropical atmosphere that are mediated by convective organization and radiative feedbacks.

2. Methodology

a. *Tropical convective rain states (CRS) and CRS rain contributions*

Self-similar tropical *convective rain states* (CRS) of organized deep convection (DeepOrg), isolated deep convection (DeepIso), and shallow convection (Shallow) are identified using spaceborne precipitation radar observations following a similar procedure that Elsaesser et al. (2010) used to define tropical precipitation types. A *k*-means clustering model is trained and applied on the statistical distribution of rain rates and echo-top heights with echo intensities > 20 dBZ in each oceanic $1° \times 1°$ latitude–longitude scene observed by precipitation radars from the Tropical Rainfall Measuring Mission (TRMM; Level 2A TRMMPR V8; Kummerow et al. 1998) exactly as in Elsaesser et al. (2010) from January 1998 to August 2014. A separate *k*-means clustering model is trained and applied on Global Precipitation Measurement (GPM; GPM KuPR V8; Hou et al. 2014) from March 2014 to December 2021 by first rescaling the clustering parameters so that their means of the 5-month overlapping period match with those in TRMM. Aside from these *convective* scenes, the residual scenes have negligible precipitation and will not be discussed in this study. Since TRMM and GPM precipitation radars cannot track convective system over time (e.g., Feng et al. 2021), how a convective system evolves is not considered when performing classification. Note that DeepOrg, DeepIso, and Shallow CRS are same as the organized deep convection, unorganized deep convection, and shallow convection clusters in Elsaesser and Kummerow (2013), and DEEP, MID-LEV, and SHAL in Elsaesser et al. (2010), respectively. These prior studies have shown that DeepOrg features mesoscale convective systems, and its apparent heating is dominated by stratiform systems with larger cold pool kinetic energy that implies stronger mesoscale downdrafts (Elsaesser et al. 2010; Elsaesser and Kummerow 2013).

Example snapshots of echo-top heights from each CRS are shown in Figs. 1a–c. In general, DeepOrg scenes have the highest echo-top heights and a larger horizontal extent of higher echo-top heights. DeepIso scenes on average include fewer pixels with the highest echo-top heights and are generally more fragmented horizontally with more isolated cores than DeepOrg. Shallow scenes, on the other hand, have generally low echo-top heights compared to DeepOrg and DeepIso scenes. In addition to echo-top heights, the algorithm also considers the ratio of convective to total rain rates. The classification method captures stronger stratiform rainfall likely from the later stage and the edge of mesoscale convective systems, as shown in some scenes in Fig. 1a with stratiform precipitation areas. Since the algorithm only considers the observed features in the precipitating pixels, some scenes with fragmented convective features are shown in Figs. 1a–c when the classification parameters are noisy due to insufficient samples. These scenes with small areas of precipitation do not affect the statistical features of CRS and are suggested to not affect their associated rainfall contribution (Elsaesser et al. 2010).

Given a spatiotemporal range, the fractional precipitation contribution of each CRS can be calculated by dividing the precipitation contributed by the scenes of each CRS by the total precipitation contributed by all CRS over that time period and region. The fractional precipitation contributed by each CRS is referred to as *CRS rain contribution*, and is denoted as f_{DeepOrg}, f_{DeepIso}, and f_{Shallow} for DeepOrg, DeepIso, and Shallow, respectively. A time length of a calendar month and $30° \times 30°$ latitude–longitude spatial domains centered at the equator that are progressively shifted by 1° longitude are used to calculate the CRS rain contributions using all the $1° \times 1°$ scenes included in each domain, as schematically shown in Fig. 1d. Each spatial domain includes more than 5000 scenes per month covered by the swaths of TRMM or GPM precipitation radar. These CRS rain contributions are available during 1998–2021, in which the values from GPM are offset by the difference between TRMM and GPM during their overlapping period such that their means match. TRMM and GPM yield consistent results such that the CRS rain contributions vary similarly over the overlapping period (not shown). Since f_{DeepOrg}, f_{DeepIso}, and f_{Shallow} are fractional

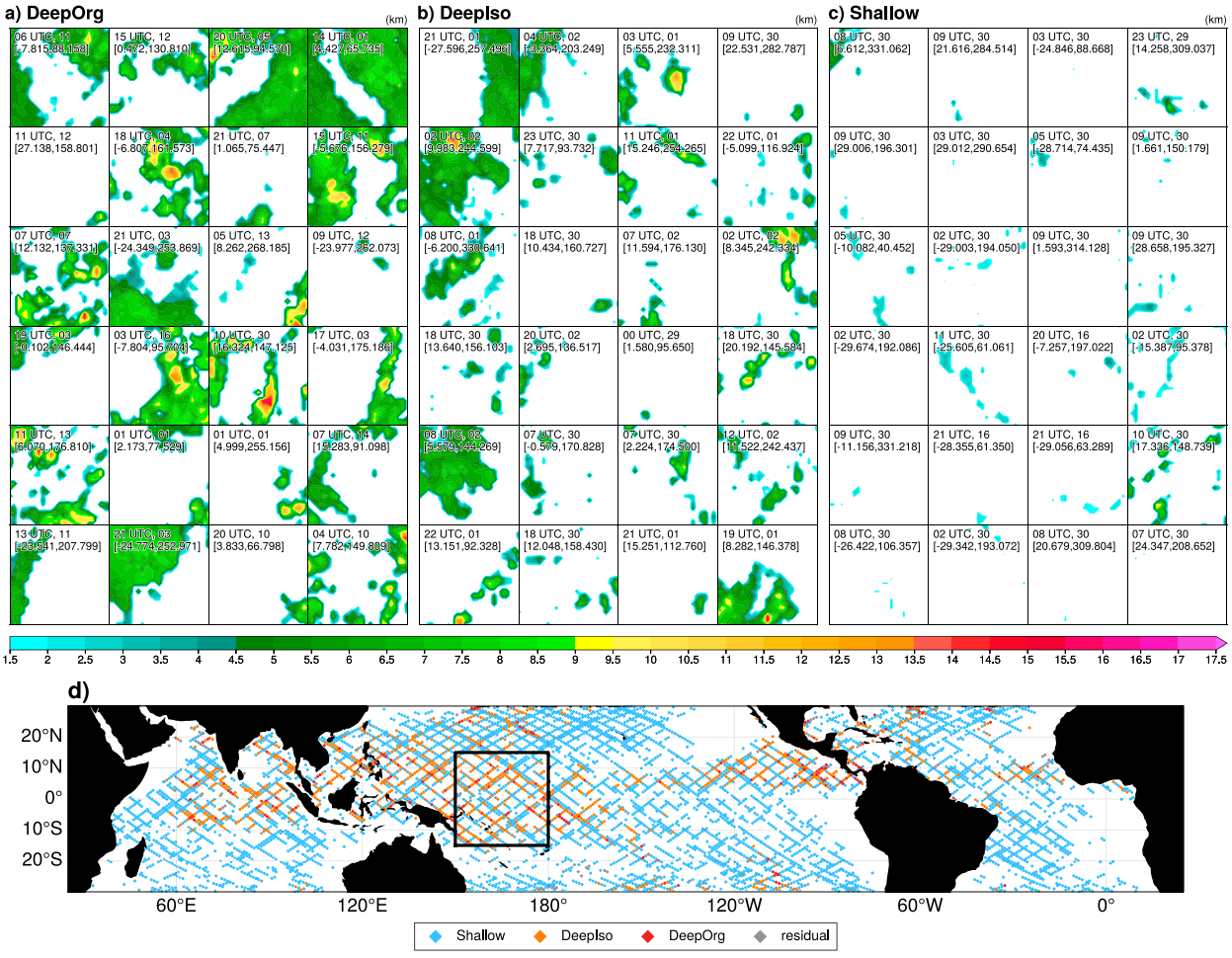

FIG. 1. Example 1° × 1° CRS scenes of echo-top heights (km) measured by TRMM during July 2012 classified as (a) DeepOrg, (b) DeepIso, and (c) Shallow. The time and day of the month (top line) and the center latitude-longitude coordinate (bottom line) of each scene is annotated at the upper-left corner. (d) Example of CRS classification over 1–5 Jul 2012, with each diamond marker roughly representing the size of a CRS scene, and the black box showing an example of the 30° × 30° domain used for averaging as described in text.

precipitation contributions, they can indicate variability in both relative frequency and intensity of convective activity associated with each CRS compared to others. Note that the large spatial domain (30° × 30°) is chosen to yield statistically stable results. A smaller spatial domain also yields qualitatively consistent conclusions, but provides noisier results (see Figs. S1–S4 in the online supplemental material for results produced for 10° × 10° domains).

Despite the gradual increase in median and mean f_{DeepOrg} with respect to SST and SST* as shown later in section 3, the *transition SST* of tropical organized deep convection is defined to quantitatively examine the "pick-up" behavior of f_{DeepOrg}. The transition SST is defined as when the median or the mean of f_{DeepOrg} within a given bin exceeds 0.3 with increasing SST above 26.5°C or increasing SST* above −1°C. The reason for selecting these SST and SST* thresholds is elaborated in section 3. The criterion of 0.3 is arbitrary and using various criteria over 0.25–0.35 does not yield different conclusions (Fig. S5). Note that the median of f_{DeepOrg} is used in SST and SST* spaces in section 3 to be compared to interquartile ranges, and the mean is used to define thresholds in SST–shear and SST*–shear space later in section 4, while using either statistic yields very similar results (not shown).

b. *Large-scale meteorological variables*

Monthly-mean large-scale meteorological variables from various data products are compared with the CRS rain contributions in this study. The SST used is from Optimum Interpolation Sea Surface Temperature version 2 (OISSTv2; Reynolds et al. 2002). SST* is calculated relative to the tropical mean defined as the mean SST between the latitudes of 15°S and 15°N. Surface precipitation is represented by the Global Precipitation Climatology Project version 2.3 product (GPCPv2.3; Adler et al. 2018). Horizontal winds on pressure levels from European Centre for Medium-Range Weather Forecasts Reanalysis v5 (ERA5; Hersbach et al. 2020) are used. The Level-3 products of the Clouds and the Earth's Radiant Energy System synoptic top of atmosphere and surface fluxes and clouds (CERES

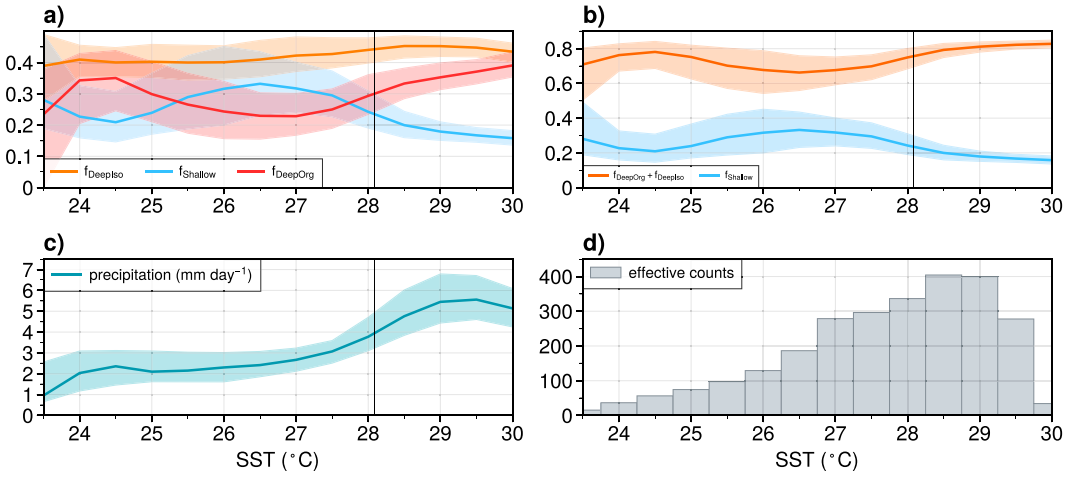

FIG. 2. The statistical distribution of (a),(b) $f_{DeepOrg}$ (red), $f_{DeepIso}$ (orange), and $f_{Shallow}$ (blue), and (c) precipitation (mm day^{-1}), binned by SST every 0.5°C, where solid lines denote the medians and shading denotes the range between the first and third quartiles, with color codes of precipitation types annotated. (d) The effective count in each SST bin. The transition SST of organized deep convection, defined at where the median $f_{DeepOrg}$ exceeds 0.30 above 26.5°C, is at 28.1°C, showing as the vertical lines in (a)–(c).

SYN1deg; Doelling et al. 2013, 2016) provide radiative heating rates on pressure levels. CERES CldTypHist provides high ice cloud properties (50–440 mb pressure; 1 mb = 1 hPa) binned by their optical depth (τ) including areal coverage, effective temperatures, and effective height for cirrus (Ci; $\tau < 3.6$), cirrostratus (Cs; $23 > \tau > 3.6$), and the upper part of cumulonimbus (Cb; $\tau > 23$).

Data are first averaged horizontally to a 1° × 1° grid. Monthly low-level wind shear magnitudes in ERA5 are calculated as the magnitude of the horizontal wind vector difference between 700 and 925 hPa ($\Delta U_{700\text{–}925}$), with the difference between 500 and 750 hPa used to define midlevel wind shear ($\Delta U_{500\text{–}750}$). Radiative heating rates are calculated using the flux divergence from the CERES SYN1deg product over oceanic regions, and are then linearly regridded vertically to the same pressure levels as ERA5. Cloud radiative heating rates are defined as the total heating rates minus the clear-sky heating rates. Data from OISSTv2, GPCPv2.3, and ERA5 are used during 1998–2021 to match the timespan of the CRS. Data from CERES SYN1deg and CldTypHist are only available during 2003–21, and are compared to other datasets only during the same range of time.

Monthly mean oceanic area averages over the 30° × 30° horizontal boxes of the variables described above are then calculated to compare to the CRS rain contributions. Oceanic regions are defined by neglecting grid points of more than 50% land area, as provided by the auxiliary data for CERES SYN1deg. Altering this threshold for land area does not substantially affect the results (not shown). The effective sample size of these averages over all oceanic regions needs to consider the overlap in space between the boxes, the different fractional area represented by each box due to land cover, and different number of days in a calendar month. Based on the above, the effective count is estimated as the actual count divided by 30 (the overlapping counts for each grid cell is 30 with the 1° longitude shift of spatial boxes), multiplied by the areal fraction of oceanic region within a box (the maximum is 1), and multiplied by the ratio of the days in a calendar month to 31 (the maximum days in a calendar month is 31). This yields effective counts of 2622 over 1998–2021 and 2074 over 2003–21, respectively. The effective counts are used as weights when calculating all the quartiles, means, and correlations between variables.

c. *El Niño–Southern Oscillation indices*

In section 3c, the dependence of results on the El Niño–Southern Oscillation (ENSO) state is discussed. The multivariate ENSO index version 2 (MEIv2; Zhang et al. 2019) is used to define ENSO events. First, the bimonthly MEIv2 is linearly interpolated to each month to match the time resolution of the other data. The warm El Niño–like months and the cold La Niña–like months are defined as when the monthly MEIv2 is greater than or equal to 0.5 (n = 35) and smaller than or equal to −0.5 (n = 89), respectively. Note that the magnitude threshold of 0.5 is used instead of 1 conventionally to ensure there are sufficient samples in both categories.

3. Tropical SST control on convection and radiative feedbacks

a. *Tropical SST and CRS rain contributions*

The relationship between CRS rain contributions and SST is explored. Figure 2a shows the statistical distribution of the fractional precipitation contributions in tropical oceanic regions binned by SST. Overall, $f_{DeepIso}$ is greater than $f_{DeepOrg}$ and $f_{Shallow}$, indicating that isolated deep convection generally makes up the greatest contribution to total precipitation at all SSTs. However, its contribution is relatively invariant across SST bins. Focusing on the medians (solid lines), $f_{DeepIso}$ is nearly constant over all SST bins at 0.4, with a slight increase with SST over 26°–28.5°C to 0.45, and a slight decrease with

SST above 28.5°C. The relative contribution to tropical precipitation from organized deep convection and from shallow convection varies more with SST. The median f_{DeepOrg} shows an increase with SST above 27°C from 0.24 to 0.39. Below this 27°C threshold, results are more complex with an increase below 24°C to 0.34, and a decrease with SST over 24.5°–27°C from 0.35 to 0.24. The median f_{Shallow} values are nearly the mirror image of median f_{DeepOrg}, which is not surprising given that all the fractional precipitation contributions add to unity. Figure 2b shows the same statistics but for the precipitation contribution by adding both deep convection types ($f_{\mathrm{DeepOrg}} + f_{\mathrm{DeepIso}}$) and for shallow convection (f_{Shallow}). The plot shows that deep convective activity as a whole ($f_{\mathrm{DeepOrg}} + f_{\mathrm{DeepIso}}$) increases with SST above 26.5°C, consistent with previous results as discussed in the section 1.

Figure 2c shows the statistical distribution of monthly-mean area-averaged tropical oceanic precipitation binned by SST. From 27° to 29.5°C, the median precipitation sharply increases with SST from 2.7 to 5.6 mm day^{-1}, associated with increase in median f_{DeepOrg} and slight increase in median f_{DeepIso}. The median precipitation increases with SST below 24.5°C to 2.4 mm day^{-1}, covarying with increasing median f_{DeepOrg}. Between 24.5° and 27°C, the median precipitation remains nearly constant at 2 mm day^{-1}, despite decreasing median f_{DeepOrg} and increasing median f_{Shallow}. The spreads of all the fractional precipitation contributions, if measured by the range between their first and third quartiles (shading), decrease with SST in the range of 27°–29.5°C. These statistical features suggest that higher precipitation tends to be produced by increasingly organized deep convection with lower variability in this relationship at higher SSTs. However, as an exception, at the highest SSTs above 29.5°C the median precipitation decreases with SST, but the large interquartile precipitation spread makes the trend uncertain, which may originate from large-scale atmospheric disturbances that controls the onset of precipitation, such as the Madden–Julian oscillation (MJO).

The increase in median f_{DeepOrg} with SST above 27°C is of interest due to its association with active tropical convection and significant precipitation as suggested by the early literature that used outgoing longwave radiative flux as a proxy for convective activity (Gadgil et al. 1984; Graham and Barnett 1987; Waliser and Graham 1993; Zhang 1993; Lau et al. 1997). Meanwhile, a nearly constant median f_{DeepIso} over all SSTs implies that most of the variation of convective activity with respect to SST observed by previous studies is from the variation in organized deep convective activity, instead of isolated deep convective activity. The definition of the transition SST of tropical organized deep convection where the median or the mean of f_{DeepOrg} exceeds 0.3 is therefore defined only when SST values are above 26.5°C, as mentioned in section 2. Our calculated transition SST for organized deep convection when conditioned on no other variables is 28.1°C (vertical lines in Figs. 2a–c). The change in transition SST with additional conditioning on vertical wind shear will be examined in section 4.

A decrease in median f_{DeepOrg} with increasing SST is observed at SST below 27°C (Fig. 2a). A possible explanation for this behavior was suggested in a numerical simulation study, in which stratiform cloud decks favored by low SST and stable atmospheres can produce radiatively driven cold pools that assist in the development of aggregated convection (Coppin and Bony 2015). However, it is not certain whether this mechanism is present in observations. This phenomenon will not be discussed further in this study and is left for future research.

b. Tropical SST and radiative feedbacks

Mesoscale organized deep convection produces larger anvils and more extensive cirrus shields compared to isolated deep convection, which impose a warming effect on the atmosphere by reducing the longwave radiative emission temperature at the top of the atmosphere. This subsection aims to study the connection between longwave radiative heating and organized deep convective activity in SST space. The radiative heating rates are first integrated over the troposphere (100–1000 mb), and then normalized by total precipitation in units of watts per square meter (W m^{-2}) to represent the contribution of longwave radiation to atmospheric heating per unit precipitation. This yields the dimensionless tropospheric radiative feedback to precipitation by longwave radiative heating under clear-sky condition ($\hat{Q}_{R,\mathrm{LW,clear}}$) and by the cloud radiative effect ($\hat{Q}_{R,\mathrm{LW,cloud}}$) defined as all-sky minus clear-sky radiative heating. For consistency, cirrus ice cloud cover is also normalized by total precipitation. The definitions of these radiative feedbacks capture how much heating is associated with a fixed amount of precipitation. Under tropical weak temperature gradient (WTG) theory, this feedback defined by radiative heating per unit surface precipitation is able to support the moistening of the atmosphere and convection through vertical advection, as widely used in studies examining convectively coupled tropical disturbances (e.g., Adames and Kim 2016; Kim et al. 2015).

Median normalized cirrus cover generally increases with SST, with a faster increase from 2.6% (mm day^{-1})$^{-1}$ at 27.5°C to 4.4% (mm day^{-1})$^{-1}$ at 30°C compared to lower SST (Fig. 3b). Median $\hat{Q}_{R,\mathrm{LW,cloud}}$ also increases with SST, which exceeds zero at around 27.5°C and exceeds 0.1 at 28.5°C (Fig. 3a). These increased feedbacks are consistent with the increase in median f_{DeepOrg} with SST (Fig. 2a), suggesting that more extensive cirrus clouds generated by more organized deep convection lead to stronger column longwave radiative heating per unit precipitation of the troposphere. This observed positive radiative feedback of organized deep convection can help maintain upward motion, as suggested by tropical WTG theory that heating must be compensated by adiabatic cooling induced by vertical motion (e.g., Sobel and Maloney 2012). Median $\hat{Q}_{R,\mathrm{LW,clear}}$ also rises with SST (Fig. 2c), which is expected given the increase in CSF with SST (Fig. 2d) and its associated clear-sky effect of enhanced water vapor trapping longwave radiative flux in the troposphere.

There are also notable heating effects from clouds and the atmosphere absorbing shortwave radiation. Positive shortwave cloud- and clear-sky radiative feedbacks are present with smaller magnitudes than in longwave radiative feedbacks (Figs. S6a,c). Thus, the total radiative feedbacks retain the same patterns as in longwave radiative feedbacks (comparing Figs. 3a,c with Figs. S6a,c), but are

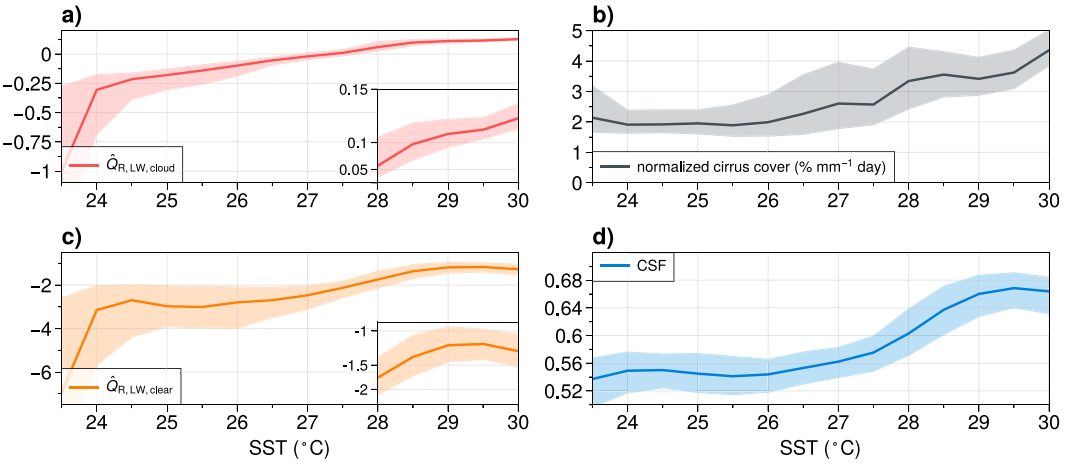

FIG. 3. As in Fig. 2a, but showing (a) $\hat{Q}_{R,LW,cloud}$ (dimensionless), (b) normalized cirrus ice cloud cover (% mm^{-1} day), (c) $\hat{Q}_{R,LW,clear}$ (dimensionless), and (d) column saturation fraction (CSF; dimensionless) with respect to liquid water. Insets with a magnified y axis at higher SST values are shown in (a) with exponential scaling and in (c) with logarithmic scaling for clarity.

slightly stronger. However, since shortwave cloud radiative heating is commonly top-heavy and associated with a cooling near the surface where the vertical moisture gradient is large (Ruppert and Hohenegger 2018), it can impose a downward motion under the WTG balance with a drying effect. The complicated interaction between the vertical structure of radiative heating and the moistening feedbacks in tropical deep convection is beyond the scope of this study.

c. *Possibly stronger control on $f_{DeepOrg}$ by SST than by SST**

To compare to previous studies suggesting that SST deviation from its tropical mean (SST*) is a better indicator of tropical precipitation than SST under both global warming trend and interannual variability (Johnson and Xie 2010; Sobel et al. 2002), similar analysis is performed by binning tropical CRS rain contributions and precipitation by SST* (Fig. 4). In SST* space, the median precipitation increases monotonically above −2.5°C (Fig. 4c), which verifies the conclusion of the previous studies. The CRS rain contributions have qualitatively similar behavior in the SST* space compared to that in the SST space (comparing Figs. 4a,b and 2a,b): median $f_{DeepIso}$ remains nearly constant; median $f_{DeepOrg}$ increases with SST* above −1°C and behaves oppositely below it; median $f_{Shallow}$ is a mirror image of median $f_{DeepOrg}$. However, the increase in median $f_{DeepOrg}$ with SST* is flatter than for SST at some high temperatures. For example, median $f_{DeepOrg}$ increases with SST* by 0.02 from 0.34 at 1°C to 0.36 at 2°C. In comparison, median $f_{DeepOrg}$ increases with SST by 0.04 from 0.33 at 28.5°C to 0.37 at 29.5°C, having twice as large increase over the same 1°C range,

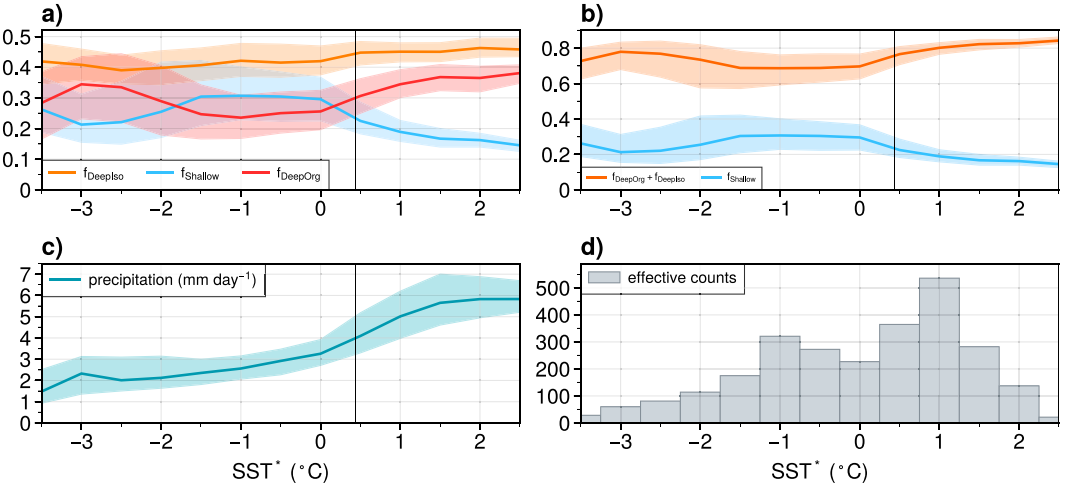

FIG. 4. As in Fig. 2, but binned by the deviation of SST from its tropical mean (SST*) every 0.5°C. The transition SST* of organized deep convection is at 0.4°C, showing as the vertical lines in (a)–(c), defined at where the median of $f_{DeepOrg}$ exceeds 0.30 above −1°C.

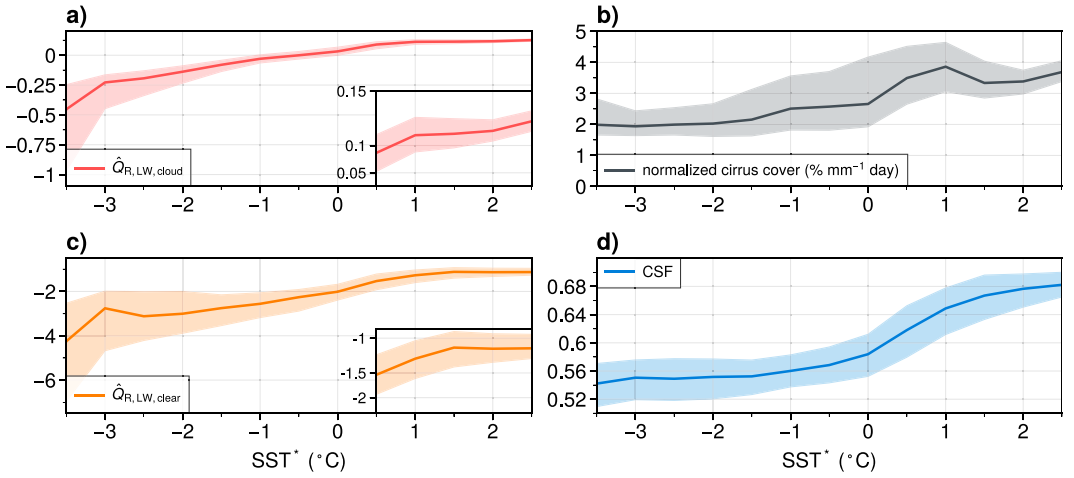

FIG. 5. As in Fig. 3, but binned by SST* every 0.5°C.

although this 0.02 excess is not very robust comparing to the magnitude of interquartile range (~0.09). The comparison suggests that while SST* is a better predictor of precipitation than SST, SST is more strongly related to organized deep convective activity than SST*. We will show in the next paragraph that this subtle difference may lead to different strengths in radiative feedback that are important for supporting convection.

Notable differences are shown in SST* space for variables related to longwave radiative feedback compared to those in SST space. Tropical precipitation increases with SST* more monotonically than with SST (Fig. 4c). Consistent with the strong coupling between tropical precipitation and column saturation fraction (CSF) (Bretherton et al. 2004), median CSF and $\hat{Q}_{R,LW,clear}$ also increase with SST* more monotonically (Figs. 5c,d). Median normalized cirrus ice cloud cover generally increases with SST* (Fig. 5b), with a relatively sudden jump from 2.7% (mm day^{-1})$^{-1}$ at 0°C to 3.9% (mm day^{-1})$^{-1}$ at 1°C, and becomes irregular above 1°C compared to that in SST space above 28.5°C. This is reflected in median $\hat{Q}_{R,LW,cloud}$, which increases with SST* below 1°C and remains relatively flatter between 1° and 2°C compared with that in SST space between 28.5° and 29.5°C (cf. the insets of Figs. 3a and 5a). This less monotonic behavior of normalized cirrus cover and longwave cloud radiative feedback in SST* space is perhaps because of the weaker increase in organized deep convective activity (measured by median $f_{DeepOrg}$) and associated anvil cloud decks at very high values of SST* versus SST, as discussed in the previous paragraph.

To summarize, it appears that while SST* is a stronger predictor of tropical precipitation, CSF, and clear-sky longwave radiative feedback, SST is a stronger predictor of tropical organized deep convective activity, normalized cirrus ice cloud cover, and longwave radiative feedback due to clouds. To support this argument, individual samples (instead of medians) are used to calculate the Pearson correlation coefficient between $\hat{Q}_{R,LW,cloud}$ and either SST above 26.5°C or SST* above −1°C, which yield 0.75 and 0.72, respectively, which are significantly different utilizing bootstrapping ($p < 0.01$). If focusing on the high-temperature conditions, the correlation coefficients obtained by SST above 28°C and SST* above 0.5°C are 0.37 and 0.22, respectively, which are also statistically different utilizing bootstrapping ($p < 0.01$). These results suggest that SST correlates better with longwave cloud radiative feedback than SST*, especially at higher surface temperatures.

We present a hypothesis for why SST more strongly controls organized deep convective activity and associated cloud radiative feedbacks than SST*. Notably, SST* has a strong control on CAPE such that it shapes the large-scale tropical circulation and free-tropospheric relative humidity patterns (e.g., Vecchi and Soden 2007). However, SST more directly controls low-level moisture content as well as its longwave radiative opacity through the Clausius–Clapeyron relationship when assuming invariant relative humidity. Since the occurrence of bifurcation in convective states depends largely on the low-level longwave radiative opacity (Emanuel et al. 2014), the organization of convection may thus vary more consistently with SST instead of SST*. A caveat of the presented hypothesis is that the radiative-convective instability discussed above requires radiative-convective equilibrium (RCE), but this is only reached nearly 65% of time on a monthly, 30° × 30° spatiotemporal scale (Jakob et al. 2019). Nevertheless, the instability may still partly contribute to convective organization, given the presence of cloud-radiative heating in ascending regions that may increase the possibility of bifurcation.

The stronger control of SST on organized deep convective activity and associated cloud radiative feedbacks can only be manifest when the SST does not covary well with SST*, which we now demonstrate to be true at higher temperatures. Figure 6a shows a bimodal structure in SST*–SST occurrence when both temperatures are high. During La Niña–like months (Fig. 6c), SST is not necessarily the highest when some of the highest values of SST* occur (blue boxes). Similarly, extremely high SST occurs while SST* is relatively low (red boxes) during El Niño–like months. It is also notable that in the green boxes, high occurrences of SST* (e.g., 0.8°C) are accompanied by a large range of SST (28°–29.5°C) during

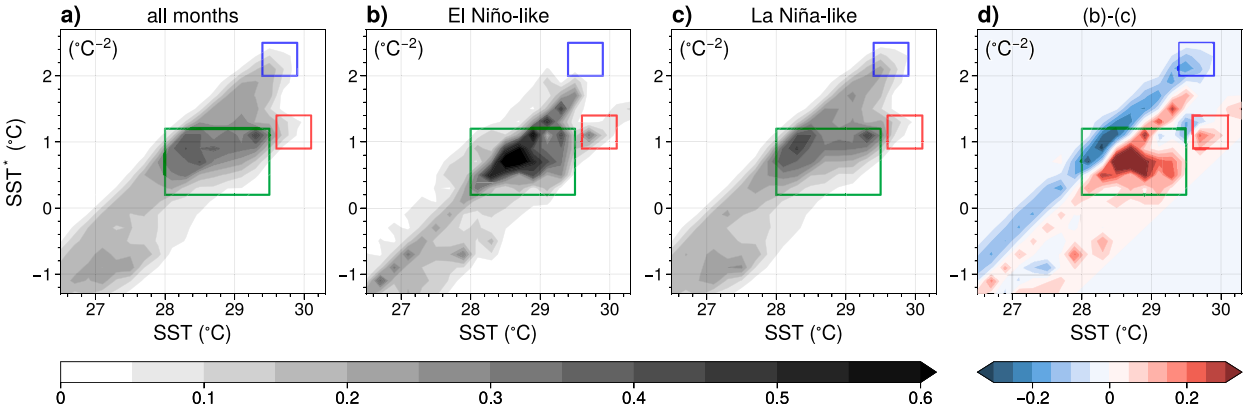

FIG. 6. The joint probability density function (°C^{-2}) of SST (x axis) and SST* (y axis) over 2003–21 in (a) all months, when (b) MEIv2 ≥ 0.5 (El Niño–like), and (c) MEIv2 ≤ 0.5 (La Niña–like). (d) The difference between the probability density function of El Niño–like and La Niña–like conditions, namely the shading of (b) minus that of (c). The reference boxes in (a)–(c) highlight the structures possibly associated with ENSO, as discussed in text.

El Niño–like months (Fig. 6b), which likely contributes to the flatter f_{DeepOrg} in SST* space than in SST space as discussed above. Additional analysis shows that the Laplacian of SST, which contributes to boundary layer convergence and divergence (Lindzen and Nigam 1987), is dependent on ENSO along the SST* axis at high SSTs above 28°C and may impose additional control on organized deep convection shown by somewhat similar patterns in Figs. S7d and S8d. However, SST as a stronger predictor is still shown when a fixed range of the magnitudes of the Laplacian of SST is selected (Figs. S9 and S10), reinforcing the robustness of SST having more control on f_{DeepOrg} than SST*.

It should be emphasized that the transition SST and SST* of deep organized convective activity is obtained from the current-state climate, and how the conclusions would hold under a different climate state is unclear. Studies have suggested that the SST that triggers tropical deep convection could vary with tropical mean SST (Johnson and Xie 2010; Hoyos and Webster 2012), which motivates our examination of SST*. However, how the tropical circulation responds to a warming climate is still an area of active investigation (e.g., Hoyos and Webster 2012; Held and Soden 2006; Knutson and Manabe 1995), and how the response of organized deep convection and associated radiative feedbacks play a role in a stronger or weaker circulation response is a topic for a future study.

4. Effects of vertical wind shear on the transition SST of f_{DeepOrg} and radiative feedbacks

a. *The transition SST of $f_{DeepOrg}$ versus low-level wind shear*

Now the focus is shifted to how nonthermodynamic factors such as low-level wind shear affect tropical f_{DeepOrg} in addition to SST. Figure 7a shows the means of f_{DeepOrg} jointly binned by SST and the low-level wind shear magnitude, defined between 700 and 925 hPa ($\Delta U_{700\text{–}925}$). This plot demonstrates a decrease in the transition SST for organized deep convection from 28.5° to 27°C as $\Delta U_{700\text{–}925}$ increases from 2 to 9 m s^{-1}. The statistical distribution of the SST near the criterion of $f_{\text{DeepOrg}} = 0.3$, obtained from data points with f_{DeepOrg} lying in the range of 0.3 ± 0.01 at given shear bins, is further depicted in Fig. 7b. The interquartile range of SST follows the decrease in its median with increasing $\Delta U_{700\text{–}925}$ up to 6 m s^{-1}, where above this the median SST stays nearly constant. This result supports the conclusion that low-level wind shear favors the development of tropical organized deep convection at constant SST, or equivalently, a higher SST is required to produce the same mean f_{DeepOrg} at weaker low-level wind shear. As noted in section 2a, the actual value of the criterion (currently 0.3) does not impact the conclusions (Fig. S5). The transition SST* of f_{DeepOrg} has similar behavior as the transition SST in SST*–$\Delta U_{700\text{–}925}$ space, but it decreases less consistently with $\Delta U_{700\text{–}925}$, supporting the conclusion that SST has stronger control on f_{DeepOrg} than SST* (Fig. S11).

Figure 7c shows the means of precipitation jointly binned by SST and $\Delta U_{700\text{–}925}$. The behavior of precipitation with respect to $\Delta U_{700\text{–}925}$ varies as a function of shear values. The mean precipitation increases with $\Delta U_{700\text{–}925}$ below the reference dividing line (dashed gray line), but with opposite behavior above it. Below the dividing line, mean precipitation covaries with mean f_{DeepOrg}, supporting the contention that more precipitation is associated with more organized deep convective activity. The increasing mean precipitation with larger $\Delta U_{700\text{–}925}$ is also consistent with the mesoscale theory that fractionally more low-level inflow into a convection system with convectively unstable air supports more intense precipitation (Alfaro 2017).

Above the dividing line, comparing Figs. 7a and 7c suggests that stronger low-level wind shear supports an increasing relative contribution of organized deep convection to precipitation, but diminishes total precipitation. Possible mechanisms for how higher $\Delta U_{700\text{–}925}$ values support f_{DeepOrg} but inhibit precipitation are suggested in the following. Strong low-level wind shear could deepen and dilute the boundary layer, leading to drying, which is unfavorable for convection plumes to maintain their buoyancy (Robe and Emanuel 2001), and

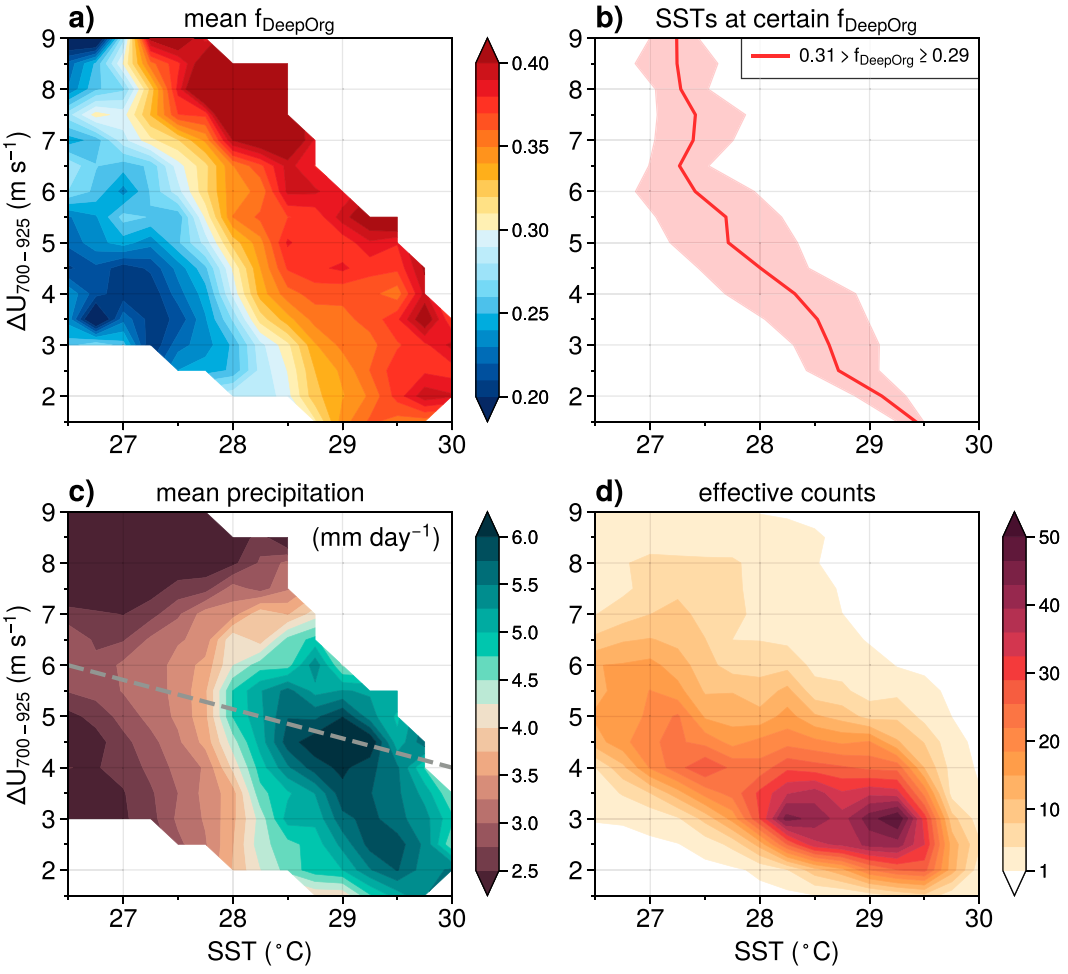

FIG. 7. (a) The means of $f_{DeepOrg}$ jointly binned by SST every 0.25°C and by $\Delta U_{700–925}$ every 0.4 m s^{-1}, where bins with effective counts less than one are omitted. The colormap in (a) is centered at 0.3, which is the criterion of the transition SST of $f_{DeepOrg}$. (b) The medians (solid line) and the range between the first and third quartiles (shading) of SST binned by $\Delta U_{700–925}$ every 0.4 m s^{-1} when $f_{DeepOrg}$ lies in 0.3 ± 0.01. (c) As in (a), but showing the mean precipitation rate (mm day^{-1}) and a reference dashed gray line as discussed further in the text. (d) As in (a), but showing the effective count in each bin.

weaken the intensity of organized convection. Figure 6 in Robe and Emanuel (2001) shows a decrease in low-level relative humidity with increasing low-level wind shear observed in cloud-resolving numerical simulations above a critical value of shear equivalent to $\Delta U_{700–925}$ value of 5 m s^{-1}, strikingly consistent with the dividing line in Fig. 6c. Rotunno et al. (1988) proposed that the shear that exceeds the "optimal state" of squall lines balancing convective cold pools causes convective cells to tilt, in a way such that the low-level air under developing cells experienced rain-induced cooling and reduced CAPE, which reduces the potential intensity of organized convection. The stronger shear that exceeds the optimal state makes convection weaker while still maintaining its persistence (Rotunno et al. 1988), consistent with the finding that mean precipitation but not $f_{DeepOrg}$ decreases at strong low-level wind shear.

b. *The transition SST of $f_{DeepOrg}$ versus midlevel wind shear*

How midlevel wind shear affects $f_{DeepOrg}$ over the tropics is also examined. First, it is shown in Fig. 8b that mean $\Delta U_{700–925}$ is largely independent of midlevel wind shear magnitudes defined between 500 and 750 hPa ($\Delta U_{500–750}$) in SST–$\Delta U_{500–750}$ space. The Pearson correlation between $\Delta U_{700–925}$ and $\Delta U_{500–750}$ is low, with a value of 0.14. This supports our motivation to examine midlevel wind shear in addition to low-level wind shear. As shown in Figs. 8a and 8c, midlevel wind shear magnitudes ($\Delta U_{500–750}$) do not have a clear effect on mean $f_{DeepOrg}$ and precipitation in SST–$\Delta U_{500–750}$ space, demonstrated by the roughly vertical contours in those mean quantities.

As SST plays the primary role controlling tropical convective organization and precipitation in Fig. 8, a question is whether the effect of midlevel wind shear is truly absent or is

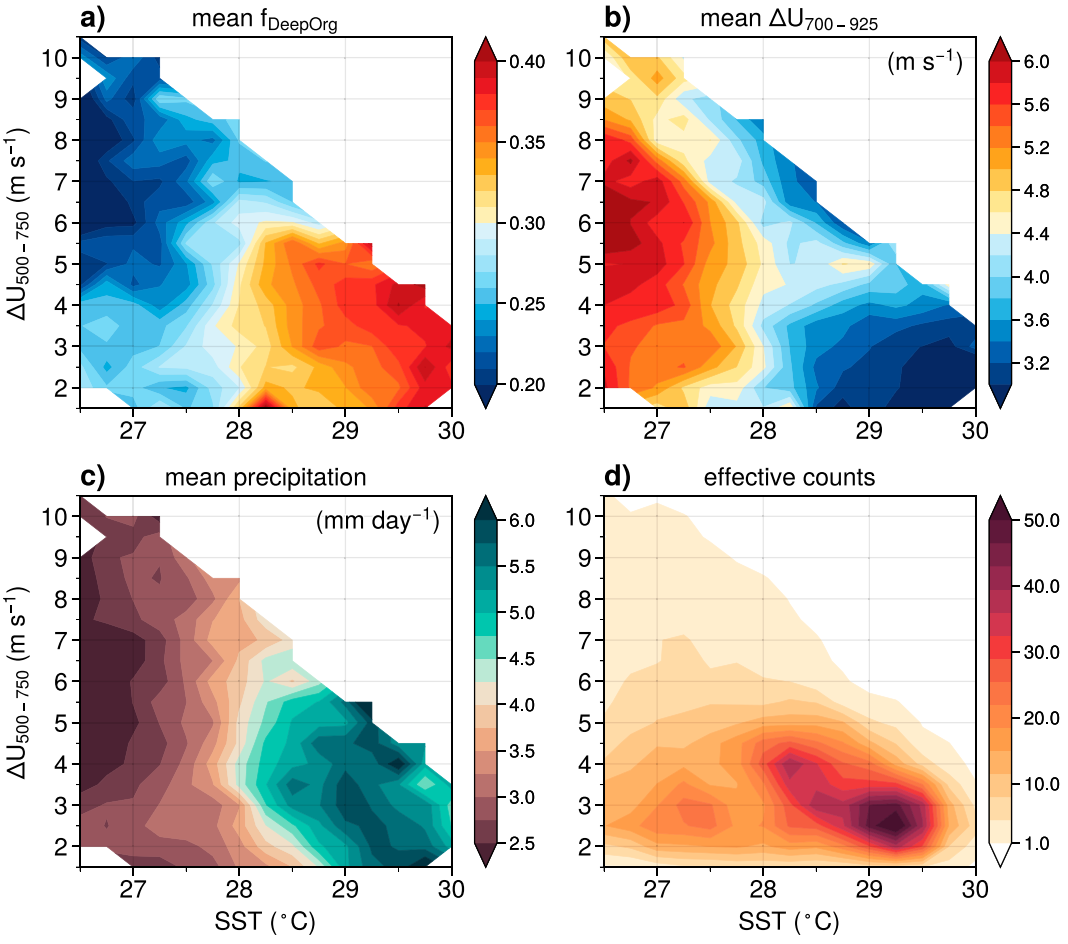

FIG. 8. As in Fig. 7, but binned by $\Delta U_{500–750}$ every 0.5 m s^{-1} instead of $\Delta U_{700–925}$ on the y axis, and the mean $\Delta U_{700–925}$ is shown in (b).

hidden in SST–$\Delta U_{500–750}$ space. When plotting the variables of interest in $\Delta U_{700–925}$–$\Delta U_{500–750}$ space, midlevel wind shear larger than 6 m s^{-1} sharply reduces the mean $f_{DeepOrg}$ to below 0.3 and mean precipitation to below 4 mm day^{-1} (Figs. 9a,c). Below $\Delta U_{500–750}$ values of 6 m s^{-1}, a complicated pattern of mean $f_{DeepOrg}$ appears in Fig. 9a, likely due to competing effects originating from the anticorrelation between mean SST and $\Delta U_{700–925}$ (Fig. 9b). With increasing $\Delta U_{700–925}$ in $\Delta U_{700–925}$–$\Delta U_{500–750}$ space, stronger low-level wind shear favors organized deep convection, but decreasing mean SST accompanied with increasing $\Delta U_{500–750}$ imposes a parallel inhibition effect.

Given the distribution of mean SST, one might conclude that high $\Delta U_{500–750}$ cuts down $f_{DeepOrg}$ and precipitation because lower SST coexists with $\Delta U_{500–750}$ above 6 m s^{-1} (Fig. 9b). However, conditions with both low $\Delta U_{500–750}$ (<6 m s^{-1}) and high $\Delta U_{700–925}$ (>5 m s^{-1}) also demonstrate much lower SST but high mean $f_{DeepOrg}$, suggesting a notable independent impact of midlevel wind shear on mean $f_{DeepOrg}$. For mean precipitation (Fig. 9c), since it mainly follows the pattern of mean SST (Fig. 9b), it cannot be concluded whether midlevel wind shear has an impact on it. This analysis implies a secondary but significant effect by strong midlevel wind shear inhibiting tropical organized deep convection compared to low-level shear and SST.

A possible physical explanation for why strong midlevel shear inhibits tropical organized deep convection is introduced here. An observational study hypothesized that very strong midlevel wind shear decouples the moisture supply of the stratiform region of a mesoscale convective system from its convective updraft, inhibiting mesoscale organization (Barnes and Houze 2013). While the study only examined this mechanism in the context of the MJO, our analysis suggests that similar physical mechanisms might be relevant on monthly time scales over global tropical oceanic regions.

c. *Cloud radiative feedback following $f_{DeepOrg}$ and vertical wind shears*

A robust control of vertical wind shear on tropical organized convection and precipitation is suggested in sections 4a and 4b. Here, we examine a possible connection between vertical wind shears and strength of the longwave radiative feedback (as defined in section 3b) associated with the precipitating convective systems.

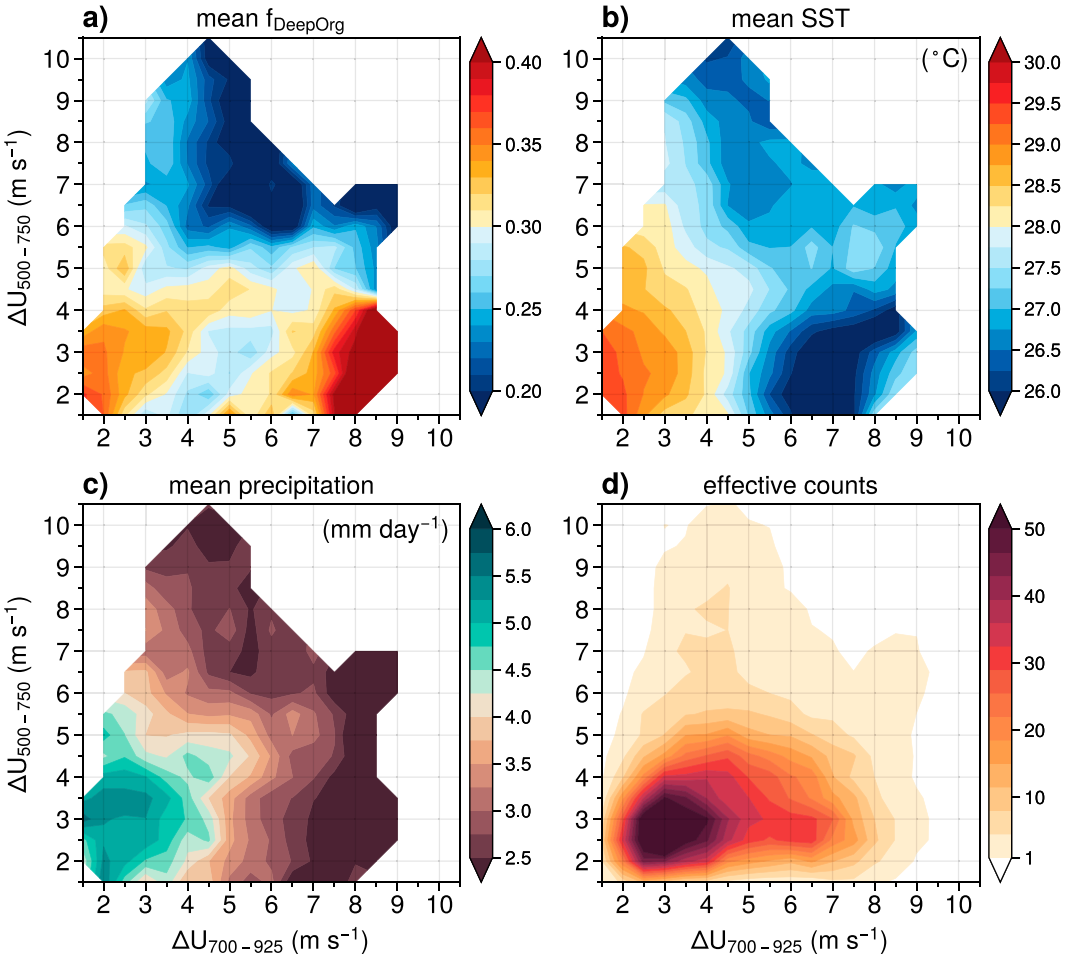

FIG. 9. As in Fig. 7, but binned by $\Delta U_{700–925}$ on the x axis and by $\Delta U_{500–750}$ on the y axis every 0.5 m s^{-1} in both axes, and the mean SST is shown in (b).

Variables related to longwave radiative heating are plotted in SST–$\Delta U_{700–925}$ space. Shading in Fig. 10a shows the tropospheric longwave cloud radiative feedback ($\hat{Q}_{R,\mathrm{LW,cloud}}$), which increases with both SST and $\Delta U_{700–925}$ and generally follows the pattern of mean f_{DeepOrg} (contours; or see Fig. 7a). Comparing Fig. 10b to Fig. 10a shows that the mean normalized cirrus cover qualitatively follows the mean $\hat{Q}_{R,\mathrm{LW,cloud}}$ as both SST and $\Delta U_{700–925}$ increase. The results suggest that more extensive anvil clouds generated by more organized deep convection produce stronger column longwave radiative heating per unit precipitation, aided by higher SST and stronger low-level wind shear in fostering convective organization. The magnitudes of mean $\hat{Q}_{R,\mathrm{LW,cloud}}$ fluctuates by ~0.1 with varying $\Delta U_{700–925}$, which may be relevant to a previous study suggesting that outgoing longwave radiation changes with vertical wind shear by the order of 10% amount of latent heat in tropical western Pacific (Lin and Mapes 2004).

However, upon closer inspection the relationship between normalized cirrus cloud cover and $\hat{Q}_{R,\mathrm{LW,cloud}}$ variations in the region of positive $\hat{Q}_{R,\mathrm{LW,cloud}}$ is not perfect, which may be attributed to changes in other high cloud types and cloud properties. Figure 11d suggests that normalized cirrostratus ice cloud cover maximizes at an SST of 28°C and $\Delta U_{700–925}$ of 7 m s^{-1}, and decreases with higher $\Delta U_{700–925}$. The mean effective temperature of cirrostratus also increases from 238.4 to 240.3 K from $\Delta U_{700–925}$ values of 7 to 8 m s^{-1} at 28°C SST (Fig. 11e), along with a decrease in mean effective cloud height (Fig. 11f), which would impose a weakening effect of cloud longwave heating with increasing low-level wind shear when cloud cover is fixed. These combined effects likely cause the $\hat{Q}_{R,\mathrm{LW,cloud}}$ to weaken at larger $\Delta U_{700–925}$, which cannot be explained by the mean normalized cirrus cover alone.

We emphasize that Fig. 11 shows the interesting finding that certain high cloud properties depend largely on low-level wind shear in addition to SST. Mean normalized cirrus cover is not only higher when SST exceeds 28°C, but also when low-level wind shear increases, a behavior especially robust above $\Delta U_{700–925}$ values of 5 m s^{-1} (Fig. 11a). Mean cirrus temperature and height varies mainly with $\Delta U_{700–925}$ in a nonlinear manner, such that temperature maximizes in a $\Delta U_{700–925}$ range of 5–7 m s^{-1} (Figs. 11b,c). As discussed in the previous paragraph, cirrostratus has a mild cloud cover change and a sudden mean temperature

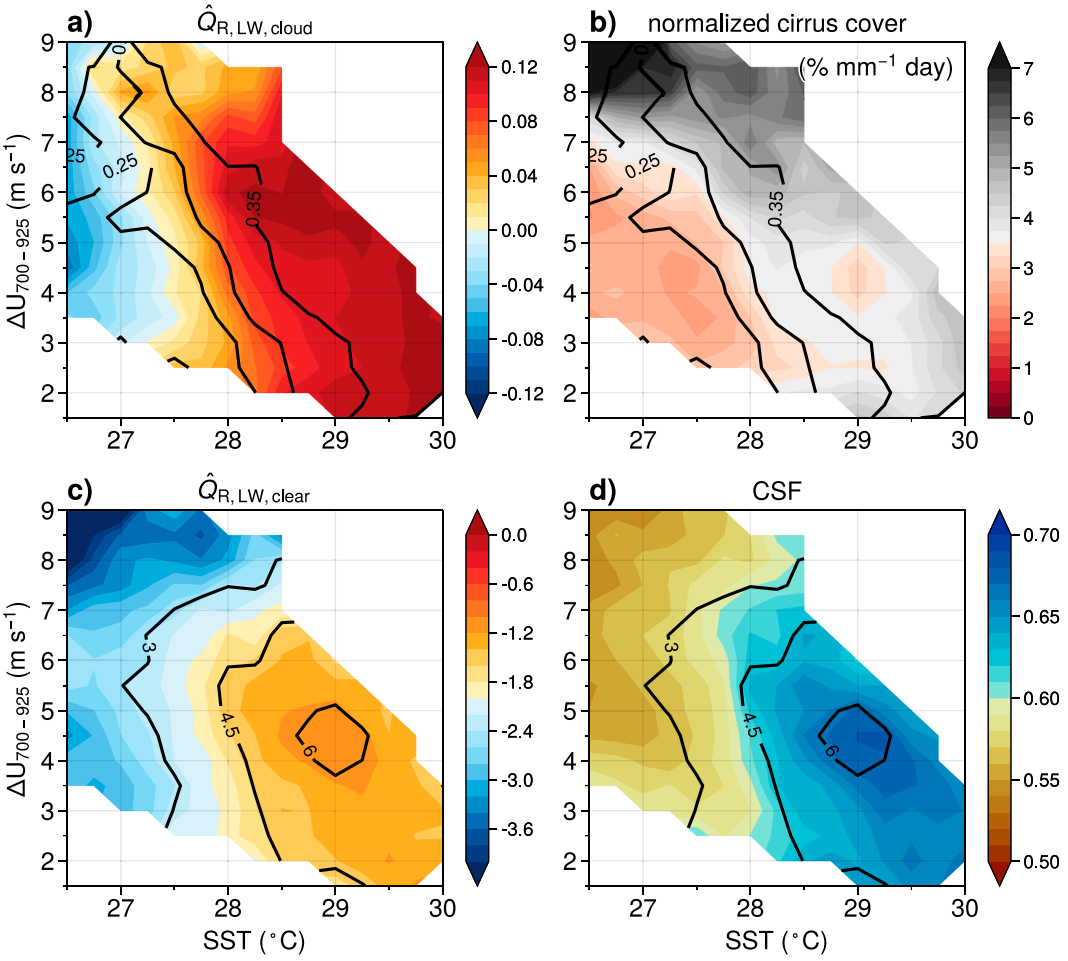

FIG. 10. As in Fig. 7a, but shading showing the means of (a) $\hat{Q}_{R,LW,cloud}$ (dimensionless), (b) normalized cirrus ice cloud area (% mm^{-1} day), (c) $\hat{Q}_{R,LW,clear}$ (dimensionless), and (d) CSF (dimensionless). Contours in (a) and (b) indicate the isolines of 0.25, 0.3, and 0.35 (as labeled) in the means of $f_{DeepOrg}$. Contours in (c) and (d) indicate the isolines of 3, 4.5, and 6 mm day^{-1} (as labeled) in the means of precipitation.

change with $\Delta U_{700–925}$ at 7 m s^{-1} (Figs. 11d,e; note the greater temperature scale in the color bar than for cirrus). Mean cumulonimbus ice cloud cover increases with low-level wind shear, especially for greater than 5 m s^{-1}, along with increasing mean cloud top temperature (Figs. 11g,h). All of these interesting dependencies of cloud types and cloud properties on SST and shear would have implications for the longwave radiation budget of the atmosphere. A detailed investigation of the interesting cloud features and resulting radiative feedbacks controlled by vertical wind shear and SST requires a separate study. Prior studies have found that stronger deep-tropospheric wind shears can contribute to an increase in cloud cover by a reduction of horizontal overlap between clouds (Saxen and Rutledge 2000; Di Giuseppe and Tompkins 2015; Sulak et al. 2020), although how low-level wind shear contributes to this effect is not clear.

Clear-sky longwave radiative feedback ($\hat{Q}_{R,LW,clear}$; shading in Fig. 10c) closely follows the moisture content of the atmosphere (shading in Fig. 10d) and mean precipitation (contours in Figs. 10c,d; or see Fig. 7c) in SST–$\Delta U_{700–925}$ space. These relationships are consistent with the clear-sky effect of enhanced water vapor trapping longwave radiative flux in the troposphere, and precipitation being closely coupled with CSF (Bretherton et al. 2004).

5. Discussion

We compare the present results to previous observational studies of convective organization. Prior studies have proposed that more-organized deep convection leads to midtropospheric drying and stronger clear-sky longwave radiative cooling (Bony et al. 2020). However, the present study shows increasing mean $\hat{Q}_{R,LW,clear}$ (i.e., decreasing cooling per unit precipitation) and CSF following higher mean $f_{DeepOrg}$, at least for shear below 6 m s^{-1} (Figs. 7c and 10c,d). Anvil cloud cover has been proposed to decrease with convection that is more organized at a fixed SST and precipitation (Stein et al. 2017), and anvil cover in an individual contiguous cloud has been shown to decrease when the underlying SST increases (Igel et al. 2014). Nonetheless, the present study shows increasing mean $\hat{Q}_{R,LW,cloud}$ and normalized cirrus ice cloud cover following higher mean

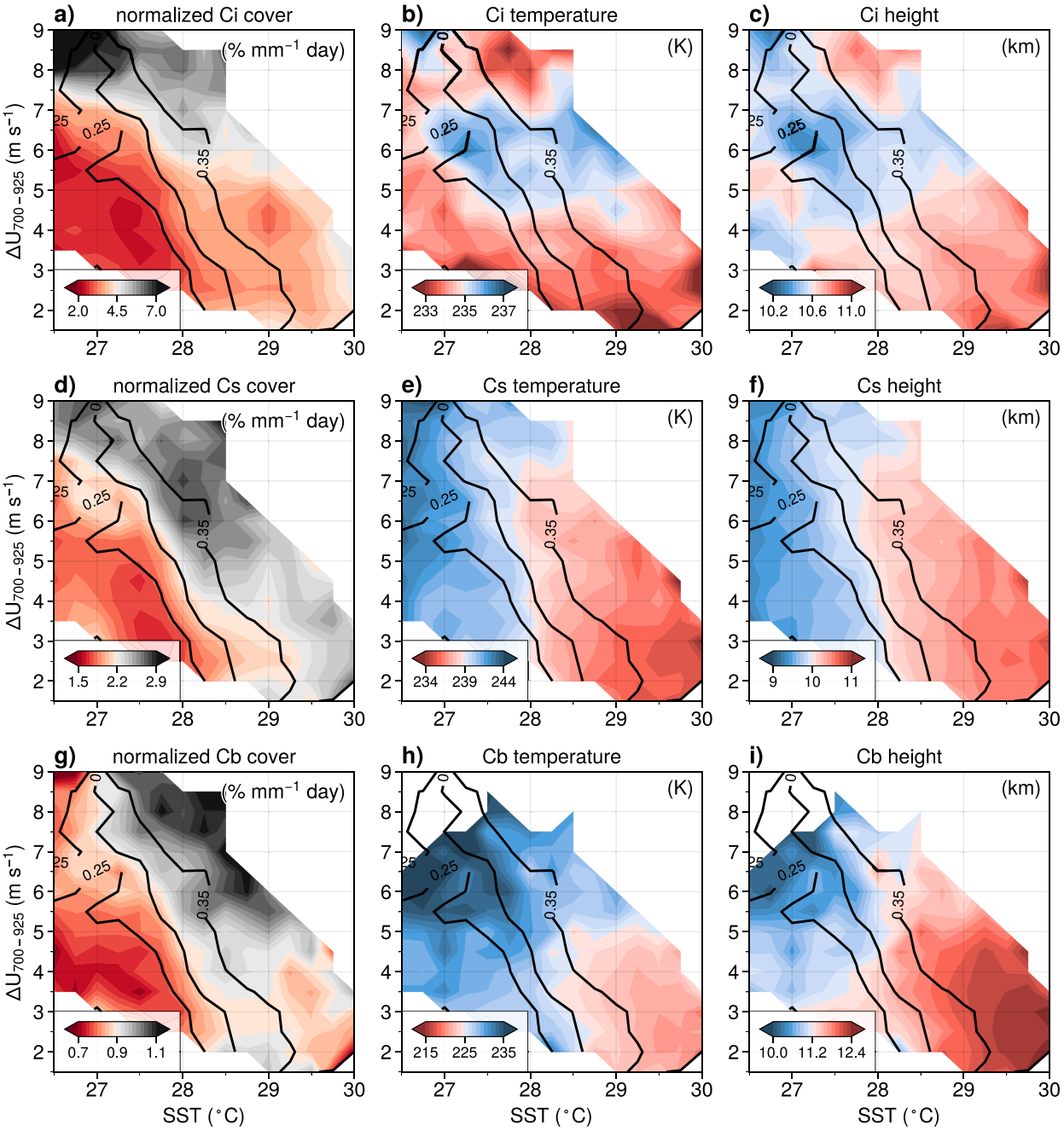

FIG. 11. As in Fig. 10b, but with shading indicating the means of (left) precipitation-normalized ice cloud cover (% mm^{-1} day), (center) effective ice cloud temperature (K), and (right) effective ice cloud height (km). Shown are (a)–(c) cirrus (Ci), (d)–(f) cirrostratus (Cs), and (g)–(i) the top part of cumulonimbus (Cb). Note that the color map of mean effective ice cloud temperature is inverted, such that warm colors indicate the stronger warming effect on the troposphere by longwave cloud radiative heating when cloud temperature is lower.

f_{DeepOrg} that increases with $\Delta U_{700-925}$ and SST (Figs. 7a and 10a,b). The discrepancies arise since quantities are measured by per unit precipitation in this study, representing the "efficiency" through which cloud covers and radiative effects are produced per unit precipitation, whereas previous studies examine the total effects. Relevantly, weaker precipitation produced by more aggregated convection at constant SST (Tobin et al. 2012) has been suggested to be an effect of not considering the anticorrelation between the area of convection and the degree of aggregation (Angulo-Umana and Kim 2023; Semie and Bony 2020). These apparent discrepancies may also partly originate from the different definitions of organized deep convection used, and from different foci on thinner cirrus and thicker anvil clouds. The literature discussed above considers the connectivity and

"clumpiness" of clouds with low brightness temperatures in 10° × 10° boxes when defining convective organization, a scale larger than contiguous convective cells. On the other hand, the present method classifies a 1° × 1° scene as organized deep convective partly when it has a high stratiform rainfall contribution (cf. Table 1 in Elsaesser et al. 2010), putting more weight on the precipitation structures that have obvious traits of mesoscale convective systems (Elsaesser and Kummerow 2013), instead of aggregation on larger spatial scales. It should be emphasized again that the 30° × 30° domains are used to obtain average rain contributions from DeepOrg scenes that have mesoscale organization traits, but not examining the aggregation on a 30° × 30° scale.

While the clustering of self-similar tropical precipitating scenes explains a large fraction (~60%) of the variability of tropical precipitation (Elsaesser et al. 2010), the unexplained ~40% also points out the limitation of the method. This is partly evident in the strong low-level shear condition discussed in section 4a, which favors deep convection being organized while diminishing mean precipitation (Fig. 7). The detailed variabilities in the horizontal shape or the intensity of organized deep convection that affect large-scale precipitation can also potentially affect radiative feedbacks, which is an important topic for future study.

In this study, monthly means over 30° × 30° domains in the tropics are examined due to limited data availability. To directly investigate the physical mechanisms discussed in this paper of how SST and vertical wind shear both affect convective organization and precipitation, such as the dynamical balance between convective cold pool and background wind profile, data with finer spatiotemporal resolution are required. It is thus desired to examine those mechanisms in a future study when data with sufficient resolution are available or by performing numerical simulations. Note that the study does not exhaustively discuss possible factors impacting tropical convective organization. Other meteorological factors, such as the presence of a coastal environment, would weaken the relationships between f_{DeepOrg}, SST, and wind shear (Fig. S12), consistent with a previous study suggesting a different CSF–precipitation relationship due to coastal processes (Bergemann and Jakob 2016).

6. Summary

The present study provides a global observational assessment of the relationships among tropical organized deep convection, precipitation, SST and SST*, vertical wind shear, and associated atmospheric radiative heating. Convective rain states (CRS) are derived using TRMM and GPM precipitation radar. The fractional contribution of organized deep convective CRS to total precipitation, f_{DeepOrg}, is used to measure tropical organized deep convective activity on monthly time scales and by 30° ×30° spatial means. As a fractional precipitation contribution, f_{DeepOrg} indicates variability in both the relative frequency and intensity of organized deep convective activity compared to other types of tropical precipitating systems.

Both SST and vertical wind shear are important regulators of tropical convective organization and precipitation. Median f_{DeepOrg} shows a pick-up behavior with respect to SST above 27°C and reaches a value of 0.3 at which the transition SST of organized deep convection is defined at 28.1°C (Fig. 2a). As organized deep convection tends to produce more anvil and cirrus clouds, precipitation-normalized cirrus ice cloud cover and tropospheric longwave cloud radiative feedbacks $\hat{Q}_{R,\mathrm{LW,cloud}}$ also increases with SST above 27°C (Figs. 3a,b), which help support upward motion associated with convective systems. Although SST* is a better indicator of tropical precipitation amount as shown in Fig. 4c and previous studies (Sobel et al. 2002), SST* has a weaker control on f_{DeepOrg} and $\hat{Q}_{R,\mathrm{LW,cloud}}$ than SST (section 3c). Particularly at higher surface temperatures, SST and SST* decouple under the influence of interannual variability such as ENSO (Fig. 6). The dependence of low-level moisture content and longwave radiative opacity on SST rather than SST*, which aids the bifurcation of convective states (Emanuel et al. 2014), may explain why tropical convective organization follows SST more than SST*.

Low-level wind shear ($\Delta U_{700\text{–}925}$) favors organized deep convective activity, evident from the transition SST of f_{DeepOrg} decreasing from 28.5° to 27°C as $\Delta U_{700\text{–}925}$ increases from 2 to 9 m s^{-1} (Figs. 7a,b), consistent with the theories of low-level wind shear helping the development of mesoscale convection (Houze 2004, and references therein). In general, longwave cloud radiative feedbacks support organized convection as shear increases, such that larger mean $\hat{Q}_{R,\mathrm{LW,cloud}}$ is present with higher $\Delta U_{700\text{–}925}$ at constant SST, following the increase in mean f_{DeepOrg} (Figs. 10a,b). Increased $\hat{Q}_{R,\mathrm{LW,cloud}}$ with higher $\Delta U_{700\text{–}925}$ and SST is mainly promoted by increased cirrus ice cloud cover per unit precipitation, but it is also shaped by complicated variations in normalized cirrostratus ice cloud cover and cloud temperature with respect to low-level wind shear (Fig. 11).

Midlevel wind shear ($\Delta U_{500\text{–}750}$) that is too strong (>6 m s^{-1}) is shown to inhibit tropical organized deep convective activity (Figs. 8 and 9). Similar conclusions were made in a previous study examining the cycle of the MJO over the Indo-Pacific warm pool, in which they suggest that a cut-off of the moisture supply from convective regions to stratiform regions occurs in organized convective systems when strong midlevel wind shear is in presence (Barnes and Houze 2013). Our result suggests that this mechanism also generally holds in the tropics on monthly time scales.

Precipitation has a more complicated relationship with vertical wind shear. When low-level wind shear is weaker, tropical mean precipitation increases with $\Delta U_{700\text{–}925}$ at constant SST, accompanied by the increase in mean f_{DeepOrg}. However, mean precipitation decreases with $\Delta U_{700\text{–}925}$ at higher low-level wind shear (Fig. 7c above the reference line). This nonlinear relationship is also shown in mean column saturation fraction (CSF) and mean longwave clear-sky radiative feedback ($\hat{Q}_{R,\mathrm{LW,clear}}$) as they are tightly connected to precipitation (Bretherton et al. 2004). It is possible that under conditions with very strong low-level wind shear, moisture in tropospheric boundary layer is diluted (Robe and Emanuel 2001), or that the shear cannot be balanced by the cold pools

produced by mesoscale convective systems (Rotunno et al. 1988), both of which could inhibit the potential intensity of convection by reducing effective CAPE while the latter mechanism still supports the presence of weaker organized convective systems that is reflected in increased mean f_{DeepOrg}.

Few observational studies have surveyed the large-scale controlling factors of organized deep convection over the global tropics. While SST is a robust indicator of large-scale convective instability, the present study demonstrates robust effects of vertical wind shear on the organization of deep convection and precipitation. These effects likely influence subsequent cloud properties and radiative feedbacks in the tropics. Differences in how global climate models represent high clouds and associated radiative heating in tropical ascending regions may contribute to spread in future tropical SST pattern projections, and could be a cause of why, for example, climate models tend to produce an El Niño–like warming pattern versus the La Niña–like tropical SST warming trend that is observed (Lee et al. 2022). The results provide an observational reference for global climate models on the relationship between large-scale meteorological conditions and cloud radiative effects, with convective organization being a possible underlying physical cause. Tropical cloud radiative feedbacks not only directly affect local radiative budgets and the maintenance of tropical variability (Adames and Maloney 2021), but also help drive circulations that affect remote parts of the globe (Hsiao et al. 2022a,b). How large-scale SST and vertical wind shear affect organization of tropical deep convection can also be compared to global cloud-resolving simulations, such as those produced by the Dynamics of the Atmospheric General Circulation Modeled on Nonhydrostatic Domains (DYAMOND) models (Stevens et al. 2019), to elucidate how biases in convection may lead to biases in global climate patterns.

Acknowledgments. This material is based upon work supported by the National Aeronautics and Space Administration under Grant 80NSSC20K1105 issued through the NASA Energy and Water Cycle Study (NEWS) and the National Science Foundation under Climate and Large-Scale Dynamics Program Grant AGS-1841754. W.-T. Hsiao is also supported by the Taiwan Ministry of Education Government Scholarship to Study Abroad (GSSA). We thank Colleen Mikovitz for processing and providing CERES SYN1deg heating rates.

Data availability statement. Monthly mean data of OISSTv2 and GPCPv2.3 are provided by the NOAA PSL, Boulder, Colorado, USA, and can be obtained from their website at https://psl.noaa.gov. CERES SYN1deg data are provided by NASA Langley Research Center, Hampton, Virginia, USA, and can be obtained from their website at https://ceres.larc.nasa.gov/data/. ERA5 data can be downloaded from https://cds.climate.copernicus.eu/. CRS and computer codes to generate the data can be downloaded at https://doi.org/10.5281/zenodo.7853386 and https://doi.org/10.5281/zenodo.7868584. Figures in this manuscript are made by ProPlot.

REFERENCES

Abbot, D. S., 2014: Resolved snowball Earth clouds. *J. Climate*, **27**, 4391–4402, https://doi.org/10.1175/JCLI-D-13-00738.1.

Adames, Á. F., and D. Kim, 2016: The MJO as a dispersive, convectively coupled moisture wave: Theory and observations. *J. Atmos. Sci.*, **73**, 913–941, https://doi.org/10.1175/JAS-D-15-0170.1.

——, and E. D. Maloney, 2021: Moisture mode theory's contribution to advances in our understanding of the Madden-Julian oscillation and other tropical disturbances. *Curr. Climate Change Rep.*, **7**, 72–85, https://doi.org/10.1007/s40641-021-00172-4.

Adler, R. F., and Coauthors, 2018: The Global Precipitation Climatology Project (GPCP) monthly analysis (new version 2.3) and a review of 2017 global precipitation. *Atmosphere*, **9**, 138, https://doi.org/10.3390/atmos9040138.

Alfaro, D. A., 2017: Low-tropospheric shear in the structure of squall lines: Impacts on latent heating under layer-lifting ascent. *J. Atmos. Sci.*, **74**, 229–248, https://doi.org/10.1175/JAS-D-16-0168.1.

Angulo-Umana, P., and D. Kim, 2023: Mesoscale convective clustering enhances tropical precipitation. *Sci. Adv.*, **9**, eabo5317, https://doi.org/10.1126/sciadv.abo5317.

Barnes, H. C., and R. A. Houze Jr., 2013: The precipitating cloud population of the Madden-Julian oscillation over the Indian and West Pacific oceans. *J. Geophys. Res. Atmos.*, **118**, 6996–7023, https://doi.org/10.1002/jgrd.50375.

Bergemann, M., and C. Jakob, 2016: How important is tropospheric humidity for coastal rainfall in the tropics? *Geophys. Res. Lett.*, **43**, 5860–5868, https://doi.org/10.1002/2016GL069255.

Bony, S., and Coauthors, 2015: Clouds, circulation and climate sensitivity. *Nat. Geosci.*, **8**, 261–268, https://doi.org/10.1038/ngeo2398.

——, B. Stevens, D. Coppin, T. Becker, K. A. Reed, A. Voigt, and B. Medeiros, 2016: Thermodynamic control of anvil cloud amount. *Proc. Natl. Acad. Sci. USA*, **113**, 8927–8932, https://doi.org/10.1073/pnas.1601472113.

——, A. Semie, R. J. Kramer, B. Soden, A. M. Tompkins, and K. A. Emanuel, 2020: Observed modulation of the tropical radiation budget by deep convective organization and lower-tropospheric stability. *AGU Adv.*, **1**, e2019AV000155, https://doi.org/10.1029/2019AV000155.

Bretherton, C. S., M. E. Peters, and L. E. Back, 2004: Relationships between water vapor path and precipitation over the tropical oceans. *J. Climate*, **17**, 1517–1528, https://doi.org/10.1175/1520-0442(2004)017<1517:RBWVPA>2.0.CO;2.

——, P. N. Blossey, and M. Khairoutdinov, 2005: An energy-balance analysis of deep convective self-aggregation above uniform SST. *J. Atmos. Sci.*, **62**, 4273–4292, https://doi.org/10.1175/JAS3614.1.

Chen, P.-J., W.-T. Chen, C.-M. Wu, and T.-S. Yo, 2021: Convective cloud regimes from a classification of object-based CloudSat observations over Asian-Australian monsoon areas. *Geophys. Res. Lett.*, **48**, e2021GL092733, https://doi.org/10.1029/2021GL092733.

Coppin, D., and S. Bony, 2015: Physical mechanisms controlling the initiation of convective self-aggregation in a general circulation model. *J. Adv. Model. Earth Syst.*, **7**, 2060–2078, https://doi.org/10.1002/2015MS000571.

Di Giuseppe, F., and A. M. Tompkins, 2015: Generalizing cloud overlap treatment to include the effect of wind shear. *J.*

Atmos. Sci., **72**, 2865–2876, https://doi.org/10.1175/JAS-D-14-0277.1.

Doelling, D. R., and Coauthors, 2013: Geostationary enhanced temporal interpolation for CERES flux products. *J. Atmos. Oceanic Technol.*, **30**, 1072–1090, https://doi.org/10.1175/JTECH-D-12-00136.1.

——, M. Sun, L. T. Nguyen, M. L. Nordeen, C. O. Haney, D. F. Keyes, and P. E. Mlynczak, 2016: Advances in geostationary-derived longwave fluxes for the CERES synoptic (SYN1deg) product. *J. Atmos. Oceanic Technol.*, **33**, 503–521, https://doi.org/10.1175/JTECH-D-15-0147.1.

Elsaesser, G. S., and C. D. Kummerow, 2013: A multisensor observational depiction of the transition from light to heavy rainfall on subdaily time scales. *J. Atmos. Sci.*, **70**, 2309–2324, https://doi.org/10.1175/JAS-D-12-0210.1.

——, ——, T. S. L'Ecuyer, Y. N. Takayabu, and S. Shige, 2010: Observed self-similarity of precipitation regimes over the tropical oceans. *J. Climate*, **23**, 2686–2698, https://doi.org/10.1175/2010JCLI3330.1.

Emanuel, K., A. A. Wing, and E. M. Vincent, 2014: Radiative-convective instability. *J. Adv. Model. Earth Syst.*, **6**, 75–90, https://doi.org/10.1002/2013MS000270.

Feng, Z., and Coauthors, 2021: A global high-resolution mesoscale convective system database using satellite-derived cloud tops, surface precipitation, and tracking. *J. Geophys. Res. Atmos.*, **126**, e2020JD034202, https://doi.org/10.1029/2020JD034202.

Gadgil, S., P. V. Joseph, and N. V. Joshi, 1984: Ocean–atmosphere coupling over monsoon regions. *Nature*, **312**, 141–143, https://doi.org/10.1038/312141a0.

Graham, N. E., and T. P. Barnett, 1987: Sea surface temperature, surface wind divergence, and convection over tropical oceans. *Science*, **238**, 657–659, https://doi.org/10.1126/science.238.4827.657.

Held, I. M., and B. J. Soden, 2006: Robust responses of the hydrological cycle to global warming. *J. Climate*, **19**, 5686–5699, https://doi.org/10.1175/JCLI3990.1.

Hersbach, H., and Coauthors, 2020: The ERA5 global reanalysis. *Quart. J. Roy. Meteor. Soc.*, **146**, 1999–2049, https://doi.org/10.1002/qj.3803.

Hou, A. Y., and Coauthors, 2014: The Global Precipitation Measurement Mission. *Bull. Amer. Meteor. Soc.*, **95**, 701–722, https://doi.org/10.1175/BAMS-D-13-00164.1.

Houze, R. A., Jr., 1989: Observed structure of mesoscale convective systems and implications for large-scale heating. *Quart. J. Roy. Meteor. Soc.*, **115**, 425–461, https://doi.org/10.1002/qj.49711548702.

——, 2004: Mesoscale convective systems. *Rev. Geophys.*, **42**, RG4003, https://doi.org/10.1029/2004RG000150.

——, K. L. Rasmussen, M. D. Zuluaga, and S. R. Brodzik, 2015: The variable nature of convection in the tropics and subtropics: A legacy of 16 years of the tropical rainfall measuring mission satellite. *Rev. Geophys.*, **53**, 994–1021, https://doi.org/10.1002/2015RG000488.

Hoyos, C. D., and P. J. Webster, 2012: Evolution and modulation of tropical heating from the last glacial maximum through the twenty-first century. *Climate Dyn.*, **38**, 1501–1519, https://doi.org/10.1007/s00382-011-1181-3.

Hsiao, W.-T., E. A. Barnes, E. D. Maloney, S. N. Tulich, J. Dias, and G. N. Kiladis, 2022a: Role of the tropics in state-dependent improvements of US West Coast NOAA Unified Forecast System precipitation forecasts. *Geophys. Res. Lett.*, **49**, e2021GL096447, https://doi.org/10.1029/2021GL096447.

——, Y.-T. Hwang, Y.-J. Chen, and S. M. Kang, 2022b: The role of clouds in shaping tropical Pacific response pattern to extratropical thermal forcing. *Geophys. Res. Lett.*, **49**, e2022GL098023, https://doi.org/10.1029/2022GL098023.

Igel, M. R., A. J. Drager, and S. C. van den Heever, 2014: A CloudSat cloud object partitioning technique and assessment and integration of deep convective anvil sensitivities to sea surface temperature. *J. Geophys. Res. Atmos.*, **119**, 10 515–10 535, https://doi.org/10.1002/2014JD021717.

Jakob, C., M. S. Singh, and L. Jungandreas, 2019: Radiative convective equilibrium and organized convection: An observational perspective. *J. Geophys. Res. Atmos.*, **124**, 5418–5430, https://doi.org/10.1029/2018JD030092.

Johnson, N. C., and S.-P. Xie, 2010: Changes in the sea surface temperature threshold for tropical convection. *Nat. Geosci.*, **3**, 842–845, https://doi.org/10.1038/ngeo1008.

Johnson, R. H., T. M. Rickenbach, S. A. Rutledge, P. E. Ciesielski, and W. H. Schubert, 1999: Trimodal characteristics of tropical convection. *J. Climate*, **12**, 2397–2418, https://doi.org/10.1175/1520-0442(1999)012<2397:TCOTC>2.0.CO;2.

Kim, D., M.-S. Ahn, I.-S. Kang, and A. D. Del Genio, 2015: Role of longwave cloud–radiation feedback in the simulation of the Madden–Julian oscillation. *J. Climate*, **28**, 6979–6994, https://doi.org/10.1175/JCLI-D-14-00767.1.

Knutson, T. R., and S. Manabe, 1995: Time-mean response over the tropical Pacific to increased CO_2 in a coupled ocean-atmosphere model. *J. Climate*, **8**, 2181–2199, https://doi.org/10.1175/1520-0442(1995)008<2181:TMROTT>2.0.CO;2.

Kummerow, C., W. Barnes, T. Kozu, J. Shiue, and J. Simpson, 1998: The Tropical Rainfall Measuring Mission (TRMM) sensor package. *J. Atmos. Oceanic Technol.*, **15**, 809–817, https://doi.org/10.1175/1520-0426(1998)015<0809:TTRMMT>2.0.CO;2.

Laing, A. G., and J. M. Fritsch, 2000: The large-scale environments of the global populations of mesoscale convective complexes. *Mon. Wea. Rev.*, **128**, 2756–2776, https://doi.org/10.1175/1520-0493(2000)128<2756:TLSEOT>2.0.CO;2.

Lau, K.-M., H.-T. Wu, and S. Bony, 1997: The role of large-scale atmospheric circulation in the relationship between tropical convection and sea surface temperature. *J. Climate*, **10**, 381–392, https://doi.org/10.1175/1520-0442(1997)010<0381:TROLSA>2.0.CO;2.

Lee, S., M. L'Heureux, A. T. Wittenberg, R. Seager, P. A. O'Gorman, and N. C. Johnson, 2022: On the future zonal contrasts of equatorial Pacific climate: Perspectives from observations, simulations, and theories. *npj Climate Atmos. Sci.*, **5**, 82, https://doi.org/10.1038/s41612-022-00301-2.

Lin, J.-L., and B. Mapes, 2004: Wind shear effects on cloud-radiation feedback in the western Pacific warm pool. *Geophys. Res. Lett.*, **31**, L16118, https://doi.org/10.1029/2004GL020199.

Lindzen, R. S., and S. Nigam, 1987: On the role of sea surface temperature gradients in forcing low-level winds and convergence in the tropics. *J. Atmos. Sci.*, **44**, 2418–2436, https://doi.org/10.1175/1520-0469(1987)044<2418:OTROSS>2.0.CO;2.

Mauritsen, T., and B. Stevens, 2015: Missing iris effect as a possible cause of muted hydrological change and high climate sensitivity in models. *Nat. Geosci.*, **8**, 346–351, https://doi.org/10.1038/ngeo2414.

Reynolds, R. W., N. A. Rayner, T. M. Smith, D. C. Stokes, and W. Wang, 2002: An improved in situ and satellite SST analysis for climate. *J. Climate*, **15**, 1609–1625, https://doi.org/10.1175/1520-0442(2002)015<1609:AIISAS>2.0.CO;2.

Robe, F. R., and K. A. Emanuel, 2001: The effect of vertical wind shear on radiative–convective equilibrium states. *J. Atmos. Sci.*, **58**, 1427–1445, https://doi.org/10.1175/1520-0469(2001)058<1427:TEOVWS>2.0.CO;2.

Roca, R., and T. Fiolleau, 2020: Extreme precipitation in the tropics is closely associated with long-lived convective systems. *Commun. Earth Environ.*, **1**, 18, https://doi.org/10.1038/s43247-020-00015-4.

Rossow, W. B., A. Mekonnen, C. Pearl, and W. Goncalves, 2013: Tropical precipitation extremes. *J. Climate*, **26**, 1457–1466, https://doi.org/10.1175/JCLI-D-11-00725.1.

Rotunno, R., J. B. Klemp, and M. L. Weisman, 1988: A theory for strong, long-lived squall lines. *J. Atmos. Sci.*, **45**, 463–485, https://doi.org/10.1175/1520-0469(1988)045<0463:ATFSLL>2.0.CO;2.

Ruppert, J. H., Jr., and C. Hohenegger, 2018: Diurnal circulation adjustment and organized deep convection. *J. Climate*, **31**, 4899–4916, https://doi.org/10.1175/JCLI-D-17-0693.1.

Saxen, T. R., and S. A. Rutledge, 2000: Surface rainfall–cold cloud fractional coverage relationship in TOGA COARE: A function of vertical wind shear. *Mon. Wea. Rev.*, **128**, 407–415, https://doi.org/10.1175/1520-0493(2000)128<0407:SRCCFC>2.0.CO;2.

Schumacher, C., R. A. Houze Jr., and I. Kraucunas, 2004: The tropical dynamical response to latent heating estimates derived from the TRMM Precipitation Radar. *J. Atmos. Sci.*, **61**, 1341–1358, https://doi.org/10.1175/1520-0469(2004)061<1341:TTDRTL>2.0.CO;2.

Semie, A. G., and S. Bony, 2020: Relationship between precipitation extremes and convective organization inferred from satellite observations. *Geophys. Res. Lett.*, **47**, e2019GL086927, https://doi.org/10.1029/2019GL086927.

Sobel, A. H., and E. Maloney, 2012: An idealized semi-empirical framework for modeling the Madden–Julian oscillation. *J. Atmos. Sci.*, **69**, 1691–1705, https://doi.org/10.1175/JAS-D-11-0118.1.

——, I. M. Held, and C. S. Bretherton, 2002: The ENSO signal in tropical tropospheric temperature. *J. Climate*, **15**, 2702–2706, https://doi.org/10.1175/1520-0442(2002)015<2702:TESITT>2.0.CO;2.

Stein, T. H. M., C. E. Holloway, I. Tobin, and S. Bony, 2017: Observed relationships between cloud vertical structure and convective aggregation over tropical ocean. *J. Climate*, **30**, 2187–2207, https://doi.org/10.1175/JCLI-D-16-0125.1.

Stevens, B., and Coauthors, 2019: DYAMOND: The DYnamics of the Atmospheric general circulation Modeled On Non-hydrostatic Domains. *Prog. Earth Planet. Sci.*, **6**, 61, https://doi.org/10.1186/s40645-019-0304-z.

Sulak, A. M., W. J. Calabrase, S. D. Ryan, and T. Heus, 2020: The contributions of shear and turbulence to cloud overlap for cumulus clouds. *J. Geophys. Res. Atmos.*, **125**, e2019JD032017, https://doi.org/10.1029/2019JD032017.

Tan, J., C. Jakob, W. B. Rossow, and G. Tselioudis, 2015: Increases in tropical rainfall driven by changes in frequency of organized deep convection. *Nature*, **519**, 451–454, https://doi.org/10.1038/nature14339.

Tobin, I., S. Bony, and R. Roca, 2012: Observational evidence for relationships between the degree of aggregation of deep convection, water vapor, surface fluxes, and radiation. *J. Climate*, **25**, 6885–6904, https://doi.org/10.1175/JCLI-D-11-00258.1.

Tsai, W.-M., and C.-M. Wu, 2017: The environment of aggregated deep convection. *J. Adv. Model. Earth Syst.*, **9**, 2061–2078, https://doi.org/10.1002/2017MS000967.

Vecchi, G. A., and B. J. Soden, 2007: Effect of remote sea surface temperature change on tropical cyclone potential intensity. *Nature*, **450**, 1066–1070, https://doi.org/10.1038/nature06423.

Waliser, D. E., and N. E. Graham, 1993: Convective cloud systems and warm-pool sea surface temperatures: Coupled interactions and self-regulation. *J. Geophys. Res.*, **98**, 12 881–12 893, https://doi.org/10.1029/93JD00872.

Wing, A. A., 2019: Self-aggregation of deep convection and its implications for climate. *Curr. Climate Change Rep.*, **5** (1), 1–11, https://doi.org/10.1007/s40641-019-00120-3.

——, K. Emanuel, C. E. Holloway, and C. Muller, 2017: Convective self-aggregation in numerical simulations: A review. *Surv. Geophys.*, **38**, 1173–1197, https://doi.org/10.1007/s10712-017-9408-4.

——, and Coauthors, 2020: Clouds and convective self-aggregation in a multimodel ensemble of radiative-convective equilibrium simulations. *J. Adv. Model. Earth Syst.*, **12**, e2020MS002138, https://doi.org/10.1029/2020MS002138.

Wolding, B., J. Dias, G. Kiladis, F. Ahmed, S. W. Powell, E. Maloney, and M. Branson, 2020: Interactions between moisture and tropical convection. Part I: The coevolution of moisture and convection. *J. Atmos. Sci.*, **77**, 1783–1799, https://doi.org/10.1175/JAS-D-19-0225.1.

Zhang, C., 1993: Large-scale variability of atmospheric deep convection in relation to sea surface temperature in the tropics. *J. Climate*, **6**, 1898–1913, https://doi.org/10.1175/1520-0442(1993)006<1898:LSVOAD>2.0.CO;2.

Zhang, T., A. Hoell, J. Perlwitz, J. Eischeid, D. Murray, M. Hoerling, and T. M. Hamill, 2019: Towards probabilistic multivariate ENSO monitoring. *Geophys. Res. Lett.*, **46**, 10 532–10 540, https://doi.org/10.1029/2019GL083946.

Zipser, E. J., D. J. Cecil, C. Liu, S. W. Nesbitt, and D. P. Yorty, 2006: Where are the most intense thunderstorms on Earth? *Bull. Amer. Meteor. Soc.*, **87**, 1057–1072, https://doi.org/10.1175/BAMS-87-8-1057.